Table 1 | Examples of MicroED structures

	Sample	Year	Resolution	Ref.	Commentary
Lysozyme (14.4 kDa)		2013	2.9 Å	7	First structure determined by electron diffraction of 3D crystals (PDB 3J4G)
Lysozyme (14.4 kDa)	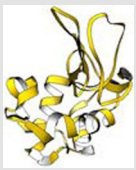	2014	2.5 Å	8	First structure determined by continuous rotation data collection, which currently is the standard MicroED method of data collection (PDB 3J6K)
Catalase (245 kDa)	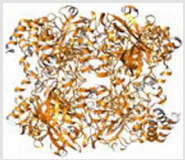	2014	3.2 Å	33	These microcrystals resisted structure determination for several decades (PDB 3J7B)
Sup35 prion protein core (905 Da)	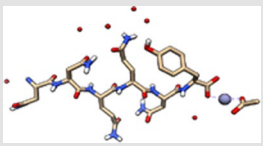	2016	1.0 Å	34	One of the first structures with phases determined by direct methods (PDB 5K2E)
Trypsin (23.4 kDa)	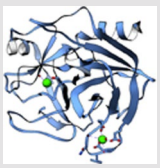	2017	1.7 Å	24	Microcrystals were generated by the fragmentation of larger crystals (PDB 5K7R)
Xylanase (21.1 kDa)		2017	2.3 Å	24	Microcrystals were generated by the fragmentation of larger crystals (PDB 5K7P)
Thaumatin (22.2 kDa)		2017	2.5 Å	24	Microcrystals were generated by the fragmentation of larger crystals (PDB 5K7Q)
TGF-β–TbRII complex (22.9 kDa)		2017	2.9 Å	24	First structure of a protein complex determined by MicroED (PDB 5TY4)
Au_{146}(p-MBA)$_{57}$ nanoparticle (37.5 kDa)	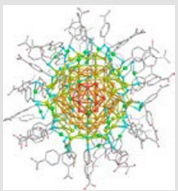	2017	0.85 Å	36	Structure of a gold nanoparticle determined by MicroED
Proteinase K (28.9 kDa)	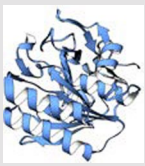	2018	1.7 Å	83	Ultra-low-dose MicroED structure (PDB 6CL7)
Bank vole prion protein segment (1.1 kDa)	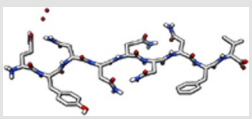	2018	0.75 Å	39	One of the highest-resolution MicroED structures to date (PDB 6AXZ)
Carbamazepine (236 Da)	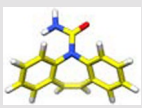	2018	0.85 Å	39, 67, 91	Structure of the drug carbamazepine as determined by MicroED

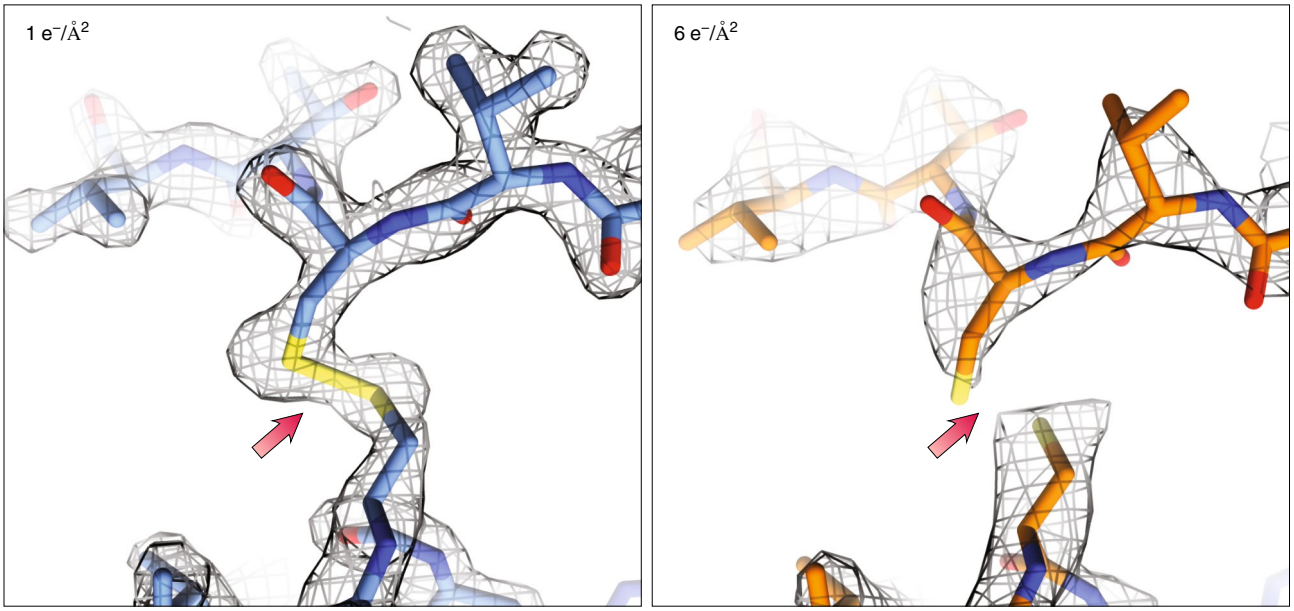

Fig. 8 | Dynamics probed in response to radiation damage. When less than 1 $e^-/Å^2$ (left) was used for structure determination of proteinase K (1.7 Å; PDB 6CL7), local radiation damage was minimal. When higher doses (right) were used (2.8 Å; PDB 6CLA), the damaging effects of the beam could be seen early on, with the breakage of disulfide bonds (red arrows) and lower attainable resolution. Density maps ($2F_o$–F_c) in gray are contoured at 1.5σ.

Phasing methods in MicroED. Most MicroED structures have been determined via molecular replacement with homologous proteins used as search models[8,23–25,48,71,83,85]. Direct methods were also successful in phasing MicroED data when the obtained resolution neared 1 Å (refs. [39,49,72]) with SHELX[86]; however, this is applicable only in cases where the samples are exceptionally well diffracting. Therefore, a welcome development would be experimental phasing methods that can be used to determine novel structures where molecular replacement is not possible but the obtainable resolution is limited to ~2–3 Å. Imaging of the crystals and tomographic reconstructions are obvious steps forward, taking advantage of the unique properties of the TEM. Using images, a moderate-resolution molecular envelope of the sample within the crystal could be determined, which then could be used to phase the MicroED data. These efforts are currently under way in several laboratories[87,88]. Heavy metal phasing is another avenue of active research. While this approach has been extremely successful in X-ray crystallography, no anomalous signal or absorption edge exists for compounds at the wavelengths of the electron microscope; therefore, only isomorphous replacement can be used for MicroED.

High-throughput small-molecule structure determination. As with biological molecules, electron diffraction can be extended to the study of organic molecules that form very small microcrystals[40,82,89–91]. Recently, a study was presented that used MicroED to determine the atomic-resolution structures of 11 small molecules[40]. These structures were determined directly from powders, with no additional crystallization optimization, and the process from sample preparation to structure solution was very quick. After the deposition of the samples onto the grid, data collection and processing were done in the same manner as described for biological crystals. The extension of MicroED to organic molecules offers a new analytical tool for studying the synthesis of new molecules. Future work that focuses on integrating the MicroED and organic synthesis pipelines promises to make this a routine method in chemistry labs.

Facilities, cameras and automation. As the use of cryo-EM methods such as MicroED becomes increasingly widespread, the need for additional centralized centers and facilities will increase. The equipment used for MicroED is essentially the same as for other cryo-EM modalities. For protein work, it is important to have an FEG, a sensitive and fast camera and, if possible, an energy filter. Camera technology is quickly progressing, and the use of direct electron detectors for MicroED is already starting. Cameras such as the Falcon3 should provide ultimate flexibility, as this camera could be used for all modalities in cryo-EM, including MicroED, whereas the other cameras appropriate for diffraction, such as the hybrid pixel detectors (for example, Timepix and EIGER[90–92]), in their current configuration are not well suited for imaging and single-particle electron microscopy.

Automation is incredibly important and will be vital for MicroED, as it has greatly improved productivity for single-particle electron microscopy. Protocols and software already have been developed for MicroED automation, including an adaptation to SerialEM[93], but a complete suite with a friendly GUI is still lacking and is currently being developed by several laboratories. In the near future, users could ship samples to the user facilities and, after sample loading, could screen and collect MicroED data remotely from their home institutions, much like what is done at most X-ray synchrotron facilities. With the current implementation of SerialEM, more than 300 datasets can be collected overnight automatically[93]. Because of the synergy among all modalities in cryo-EM user facilities, we expect that MicroED will have a broad impact on structural biology in the coming decades.

Received: 14 July 2018; Accepted: 25 March 2019;
Published online: 29 April 2019

References

1. Cheng, Y., Grigorieff, N., Penczek, P. A. & Walz, T. A primer to single-particle cryo-electron microscopy. *Cell* **161**, 438–449 (2015).
2. Beck, M. & Baumeister, W. Cryo-electron tomography: can it reveal the molecular sociology of cells in atomic detail? *Trends Cell Biol.* **26**, 825–837 (2016).
3. Wisedchaisri, G., Reichow, S. L. & Gonen, T. Advances in structural and functional analysis of membrane proteins by electron crystallography. *Structure* **19**, 1381–1393 (2011).

4. Glaeser, R. M. Review: electron crystallography: present excitement, a nod to the past, anticipating the future. *J. Struct. Biol.* **128**, 3–14 (1999).
5. Nannenga, B. L. & Gonen, T. MicroED opens a new era for biological structure determination. *Curr. Opin. Struct. Biol.* **40**, 128–135 (2016).
6. Rodriguez, J. A., Eisenberg, D. S. & Gonen, T. Taking the measure of MicroED. *Curr. Opin. Struct. Biol.* **46**, 79–86 (2017).
7. Shi, D., Nannenga, B. L., Iadanza, M. G. & Gonen, T. Three-dimensional electron crystallography of protein microcrystals. *eLife* **2**, e01345 (2013).
8. Nannenga, B. L., Shi, D., Leslie, A. G. W. & Gonen, T. High-resolution structure determination by continuous-rotation data collection in MicroED. *Nat. Methods* **11**, 927–930 (2014).
This work introduced the 'continuous rotation' method of MicroED data collection, which is currently the standard procedure for data collection.
9. Gonen, T., Sliz, P., Kistler, J., Cheng, Y. & Walz, T. Aquaporin-0 membrane junctions reveal the structure of a closed water pore. *Nature* **429**, 193–197 (2004).
10. Gonen, T. et al. Lipid-protein interactions in double-layered two-dimensional AQP0 crystals. *Nature* **438**, 633–638 (2005).
11. Henderson, R. & Unwin, P. N. Three-dimensional model of purple membrane obtained by electron microscopy. *Nature* **257**, 28–32 (1975).
12. Henderson, R. et al. Model for the structure of bacteriorhodopsin based on high-resolution electron cryo-microscopy. *J. Mol. Biol.* **213**, 899–929 (1990).
13. Grigorieff, N., Ceska, T. A., Downing, K. H., Baldwin, J. M. & Henderson, R. Electron-crystallographic refinement of the structure of bacteriorhodopsin. *J. Mol. Biol.* **259**, 393–421 (1996).
14. Subramaniam, S. & Henderson, R. Crystallographic analysis of protein conformational changes in the bacteriorhodopsin photocycle. *Biochim. Biophys. Acta* **1460**, 157–165 (2000).
15. Kühlbrandt, W., Wang, D. N. & Fujiyoshi, Y. Atomic model of plant light-harvesting complex by electron crystallography. *Nature* **367**, 614–621 (1994).
16. Unwin, P. N. & Henderson, R. Molecular structure determination by electron microscopy of unstained crystalline specimens. *J. Mol. Biol.* **94**, 425–440 (1975).
17. Dorset, D. L. & Parsons, D. F. Electron-diffraction from single, fully-hydrated, ox liver catalase microcrystals. *Acta Crystallogr. A* **31**, 210–215 (1975).
18. Dorset, D. L. & Parsons, D. F. Thickness measurements of wet protein crystals in electron-microscope. *J. Appl. Crystallogr.* **8**, 12–14 (1975).
19. Taylor, K. A. & Glaeser, R. M. Electron microscopy of frozen hydrated biological specimens. *J. Ultrastruct. Res.* **55**, 448–456 (1976).
20. Jiang, L., Georgieva, D., Zandbergen, H. W. & Abrahams, J. P. Unit-cell determination from randomly oriented electron-diffraction patterns. *Acta Crystallogr. D Biol. Crystallogr.* **65**, 625–632 (2009).
21. Nederlof, I., van Genderen, E., Li, Y. W. & Abrahams, J. P. A Medipix quantum area detector allows rotation electron diffraction data collection from submicrometre three-dimensional protein crystals. *Acta Crystallogr. D Biol. Crystallogr.* **69**, 1223–1230 (2013).
22. Iadanza, M. G. & Gonen, T. A suite of software for processing MicroED data of extremely small protein crystals. *J. Appl. Crystallogr.* **47**, 1140–1145 (2014).
23. Hattne, J., Shi, D., de la Cruz, M. J., Reyes, F. E. & Gonen, T. Modeling truncated pixel values of faint reflections in MicroED images. *J. Appl. Crystallogr.* **49**, 1029–1034 (2016).
24. de la Cruz, M. J. et al. Atomic-resolution structures from fragmented protein crystals with the cryoEM method MicroED. *Nat. Methods* **14**, 399–402 (2017).
Here several methods for the fragmentation of larger, and in some cases poorly ordered, crystals into microcrystals suitable for MicroED are described.
25. Luo, F. et al. Atomic structures of FUS LC domain segments reveal bases for reversible amyloid fibril formation. *Nat. Struct. Mol. Biol.* **25**, 341–346 (2018).
26. Duyvesteyn, H. M. E. et al. Machining protein microcrystals for structure determination by electron diffraction. *Proc. Natl Acad. Sci. USA* **115**, 9569–9573 (2018).
27. Kolb, U., Mugnaioli, E. & Gorelik, T. E. Automated electron diffraction tomography—a new tool for nano crystal structure analysis. *Cryst. Res. Technol.* **46**, 542–554 (2011).
28. Wan, W., Sun, J., Su, J., Hovmöller, S. & Zou, X. Three-dimensional rotation electron diffraction: software *RED* for automated data collection and data processing. *J. Appl. Crystallogr.* **46**, 1863–1873 (2013).
29. Mugnaioli, E. et al. Ab initio structure determination of vaterite by automated electron diffraction. *Angew. Chem. Int. Ed. Engl.* **51**, 7041–7045 (2012).
30. Feyand, M. et al. Automated diffraction tomography for the structure elucidation of twinned, sub-micrometer crystals of a highly porous, catalytically active bismuth metal-organic framework. *Angew. Chem. Int. Ed. Engl.* **51**, 10373–10376 (2012).
31. Jiang, J. et al. Synthesis and structure determination of the hierarchical meso-microporous zeolite ITQ-43. *Science* **333**, 1131–1134 (2011).
32. Gorelik, T. E., Stewart, A. A. & Kolb, U. Structure solution with automated electron diffraction tomography data: different instrumental approaches. *J. Microsc.* **244**, 325–331 (2011).
33. Mugnaioli, E., Gorelik, T. & Kolb, U. "Ab initio" structure solution from electron diffraction data obtained by a combination of automated diffraction tomography and precession technique. *Ultramicroscopy* **109**, 758–765 (2009).
34. Simancas, J. et al. Ultrafast electron diffraction tomography for structure determination of the new zeolite ITQ-58. *J. Am. Chem. Soc.* **138**, 10116–10119 (2016).
35. Zhang, C. et al. An extra-large-pore zeolite with 24×8×8-ring channels using a structure-directing agent derived from traditional Chinese medicine. *Angew. Chem. Int. Ed. Engl.* **57**, 6486–6490 (2018).
36. Zhang, Y. B. et al. Single-crystal structure of a covalent organic framework. *J. Am. Chem. Soc.* **135**, 16336–16339 (2013).
37. Shi, D. et al. The collection of MicroED data for macromolecular crystallography. *Nat. Protoc.* **11**, 895–904 (2016).
Detailed protocols for the collection of MicroED data. New users are encouraged to read these protocols prior to using MicroED.
38. Hattne, J. et al. MicroED data collection and processing. *Acta Crystallogr. A Found. Adv.* **71**, 353–360 (2015).
39. Gallagher-Jones, M. et al. Sub-ångström cryo-EM structure of a prion protofibril reveals a polar clasp. *Nat. Struct. Mol. Biol.* **25**, 131–134 (2018).
40. Jones, C. G. et al. The cryoEM method MicroED as a powerful tool for small molecule structure determination. *ACS Cent. Sci.* **4**, 1587–1592 (2018).
41. Vergara, S. et al. MicroED structure of Au_{146}(p-MBA)$_{57}$ at subatomic resolution reveals a twinned FCC cluster. *J. Phys. Chem. Lett.* **8**, 5523–5530 (2017).
42. Fromme, P. & Spence, J. C. Femtosecond nanocrystallography using X-ray lasers for membrane protein structure determination. *Curr. Opin. Struct. Biol.* **21**, 509–516 (2011).
43. Smith, J. L., Fischetti, R. F. & Yamamoto, M. Micro-crystallography comes of age. *Curr. Opin. Struct. Biol.* **22**, 602–612 (2012).
44. Yamamoto, M. et al. Protein microcrystallography using synchrotron radiation. *IUCrJ* **4**, 529–539 (2017).
45. Martin-Garcia, J. M., Conrad, C. E., Coe, J., Roy-Chowdhury, S. & Fromme, P. Serial femtosecond crystallography: a revolution in structural biology. *Arch. Biochem. Biophys.* **602**, 32–47 (2016).
46. Spence, J. C. H. X-ray lasers for structure and dynamics in biology. *IUCrJ* **5**, 236–237 (2018).
47. Henderson, R. The potential and limitations of neutrons, electrons and X-rays for atomic resolution microscopy of unstained biological molecules. *Q. Rev. Biophys.* **28**, 171–193 (1995).
48. Nannenga, B. L., Shi, D., Hattne, J., Reyes, F. E. & Gonen, T. Structure of catalase determined by MicroED. *eLife* **3**, e03600 (2014).
49. Sawaya, M. R. et al. Ab initio structure determination from prion nanocrystals at atomic resolution by MicroED. *Proc. Natl Acad. Sci. USA* **113**, 11232–11236 (2016).
The first structure determined by MicroED that was phased experimentally. In this study, the high-resolution and MicroED data quality allowed structure solution by direct methods.
50. Krotee, P. et al. Atomic structures of fibrillar segments of hIAPP suggest tightly mated β-sheets are important for cytotoxicity. *eLife* **6**, e19273 (2017).
51. Seidler, P. M. et al. Structure-based inhibitors of tau aggregation. *Nat. Chem.* **10**, 170–176 (2018).
52. Hughes, M. P. et al. Atomic structures of low-complexity protein segments reveal kinked β sheets that assemble networks. *Science* **359**, 698–701 (2018).
53. Kissick, D. J., Wanapun, D. & Simpson, G. J. Second-order nonlinear optical imaging of chiral crystals. *Annu. Rev. Anal. Chem. (Palo Alto Calif.)* **4**, 419–437 (2011).
54. Stevenson, H. P. et al. Use of transmission electron microscopy to identify nanocrystals of challenging protein targets. *Proc. Natl Acad. Sci. USA* **111**, 8470–8475 (2014).
55. Barnes, C. O. et al. Assessment of microcrystal quality by transmission electron microscopy for efficient serial femtosecond crystallography. *Arch. Biochem. Biophys.* **602**, 61–68 (2016).
56. Stevenson, H. P. et al. Transmission electron microscopy for the evaluation and optimization of crystal growth. *Acta Crystallogr. D Struct. Biol.* **72**, 603–615 (2016).
57. Martynowycz, M. W., Zhao, W., Hattne, J., Jensen, G. J. & Gonen, T. Collection of continuous rotation MicroED data from ion beam-milled crystals of any size. *Structure* **27**, 545–548 (2019).
58. Gonen, T. The collection of high-resolution electron diffraction data. *Methods Mol. Biol.* **955**, 153–169 (2013).
59. Leslie, A. G. W. & Powell, H. R. Processing diffraction data with mosflm. In *Evolving Methods for Macromolecular Crystallography* (eds. Read, R. J. & Sussman, J. L.) 41–51 (Springer, 2007).

60. Battye, T. G., Kontogiannis, L., Johnson, O., Powell, H. R. & Leslie, A. G. iMOSFLM: a new graphical interface for diffraction-image processing with MOSFLM. *Acta Crystallogr. D Biol. Crystallogr.* **67**, 271–281 (2011).
61. Kabsch, W. XDS. *Acta Crystallogr. D Biol. Crystallogr.* **66**, 125–132 (2010).
62. Otwinowski, Z. & Minor, W. Processing of X-ray diffraction data collected in oscillation mode. *Methods Enzymol.* **276**, 307–326 (1997).
63. Waterman, D. G. et al. The DIALS framework for integration software. *CCP4 Newsl. Protein Crystallogr.* **49**, 16–19 (2013).
64. Clabbers, M. T. B., Gruene, T., Parkhurst, J. M., Abrahams, J. P. & Waterman, D. G. Electron diffraction data processing with DIALS. *Acta Crystallogr. D Struct. Biol.* **74**, 506–518 (2018).
65. Winn, M. D. et al. Overview of the CCP4 suite and current developments. *Acta Crystallogr. D Biol. Crystallogr.* **67**, 235–242 (2011).
66. Adams, P. D. et al. PHENIX: a comprehensive Python-based system for macromolecular structure solution. *Acta Crystallogr. D Biol. Crystallogr.* **66**, 213–221 (2010).
67. Murshudov, G. N., Vagin, A. A. & Dodson, E. J. Refinement of macromolecular structures by the maximum-likelihood method. *Acta Crystallogr. D Biol. Crystallogr.* **53**, 240–255 (1997).
68. Balbirnie, M., Grothe, R. & Eisenberg, D. S. An amyloid-forming peptide from the yeast prion Sup35 reveals a dehydrated beta-sheet structure for amyloid. *Proc. Natl Acad. Sci. USA* **98**, 2375–2380 (2001).
69. Nelson, R. et al. Structure of the cross-beta spine of amyloid-like fibrils. *Nature* **435**, 773–778 (2005).
70. Sawaya, M. R. et al. Atomic structures of amyloid cross-beta spines reveal varied steric zippers. *Nature* **447**, 453–457 (2007).
71. Rodriguez, J. A. et al. Structure of the toxic core of α-synuclein from invisible crystals. *Nature* **525**, 486–490 (2015).
First novel structure determined by MicroED. This work paved the way for the many new peptide structures from amyloidogenic proteins.
72. Guenther, E. L. et al. Atomic structures of TDP-43 LCD segments and insights into reversible or pathogenic aggregation. *Nat. Struct. Mol. Biol.* **25**, 463–471 (2018).
73. Krotee, P. et al. Common fibrillar spines of amyloid-β and human islet amyloid polypeptide revealed by microelectron diffraction and structure-based inhibitors. *J. Biol. Chem.* **293**, 2888–2902 (2018).
74. Purdy, M. D. et al. MicroED structures of HIV-1 Gag CTD-SP1 reveal binding interactions with the maturation inhibitor bevirimat. *Proc. Natl Acad. Sci. USA* **115**, 13258–13263 (2018).
75. Wagner, J. M. et al. Crystal structure of an HIV assembly and maturation switch. *eLife* **5**, e17063 (2016).
76. Schmidt, M. Mix and inject: reaction initiation by diffusion for time-resolved macromolecular crystallography. *Adv. Condens. Matter Phys.* **2013**, 167276 (2013).
77. Unwin, N. & Fujiyoshi, Y. Gating movement of acetylcholine receptor caught by plunge-freezing. *J. Mol. Biol.* **422**, 617–634 (2012).
78. Berriman, J. & Unwin, N. Analysis of transient structures by cryo-microscopy combined with rapid mixing of spray droplets. *Ultramicroscopy* **56**, 241–252 (1994).
79. Unwin, N. Acetylcholine receptor channel imaged in the open state. *Nature* **373**, 37–43 (1995).
80. Nogly, P. et al. Retinal isomerization in bacteriorhodopsin captured by a femtosecond x-ray laser. *Science* **361**, eaat0094 (2018).
81. Pande, K. et al. Femtosecond structural dynamics drives the trans/cis isomerization in photoactive yellow protein. *Science* **352**, 725–729 (2016).
82. Wu, J. S. & Spence, J. C. Structure and bonding in alpha-copper phthalocyanine by electron diffraction. *Acta Crystallogr. A* **59**, 495–505 (2003).
83. Hattne, J. et al. Analysis of global and site-specific radiation damage in cryo-EM. *Structure* **26**, 759–766 (2018).
84. Garman, E. F. Radiation damage in macromolecular crystallography: what is it and why should we care? *Acta Crystallogr. D Biol. Crystallogr.* **66**, 339–351 (2010).
85. Nannenga, B. L., Iadanza, M. G., Vollmar, B. S. & Gonen, T. Overview of electron crystallography of membrane proteins: crystallization and screening strategies using negative stain electron microscopy. *Curr. Protoc. Protein Sci.* **72**, 17.15.1–17.15.11 (2013).
86. Sheldrick, G. M. A short history of SHELX. *Acta Crystallogr. A* **64**, 112–122 (2008).
87. Nederlof, I., Li, Y. W., van Heel, M. & Abrahams, J. P. Imaging protein three-dimensional nanocrystals with cryo-EM. *Acta Crystallogr. D Biol. Crystallogr.* **69**, 852–859 (2013).
88. van Genderen, E., Li, Y. W., Nederlof, I. & Abrahams, J. P. Lattice filter for processing image data of three-dimensional protein nanocrystals. *Acta Crystallogr. D Struct. Biol.* **72**, 34–39 (2016).
89. Gorelik, T. E., van de Streek, J., Kilbinger, A. F., Brunklaus, G. & Kolb, U. Ab-initio crystal structure analysis and refinement approaches of oligo p-benzamides based on electron diffraction data. *Acta Crystallogr. B* **68**, 171–181 (2012).
90. Gruene, T. et al. Rapid structure determination of microcrystalline molecular compounds using electron diffraction. *Angew. Chem. Int. Ed. Engl.* **57**, 16313–16317 (2018).
91. van Genderen, E. et al. Ab initio structure determination of nanocrystals of organic pharmaceutical compounds by electron diffraction at room temperature using a Timepix quantum area direct electron detector. *Acta Crystallogr. A Found. Adv.* **72**, 236–242 (2016).
92. Clabbers, M. T. B. et al. Protein structure determination by electron diffraction using a single three-dimensional nanocrystal. *Acta Crystallogr. D Struct. Biol.* **73**, 738–748 (2017).
93. de la Cruz, M. J., Martynowycz, M. W., Hattne, J. & Gonen, T. MicroED data collection with SerialEM. *Ultramicroscopy* **201**, 77–80 (2019).
94. Fernández-Busnadiego, R. et al. Insights into the molecular organization of the neuron by cryo-electron tomography. *J. Electron Microsc. (Tokyo)* **60**, S137–S148 (2011).
95. Bartesaghi, A. et al. 2.2 Å resolution cryo-EM structure of β-galactosidase in complex with a cell-permeant inhibitor. *Science* **348**, 1147–1151 (2015).
96. Liu, S. & Gonen, T. MicroED structure of the NaK ion channel reveals a Na^+ partition process into the selectivity filter. *Commun. Biol.* **1**, 38 (2018).
The first membrane protein determined by continuous rotation MicroED.
97. Subramanian, G., Basu, S., Liu, H., Zuo, J. M. & Spence, J. C. H. Solving protein nanocrystals by cryo-EM diffraction: multiple scattering artifacts. *Ultramicroscopy* **148**, 87–93 (2015).
98. Vincent, R. & Midgley, P. A. Double conical beam-rocking system for measurement of integrated electron diffraction intensities. *Ultramicroscopy* **53**, 271–282 (1994).
99. Midgley, P. A. & Eggeman, A. S. Precession electron diffraction—a topical review. *IUCrJ* **2**, 126–136 (2015).
100. Gjonnes, J. et al. Structure model for the phase AlmFe derived from three-dimensional electron diffraction intensity data collected by a precession technique. Comparison with convergent-beam diffraction. *Acta Crystallogr. A* **54**, 306–319 (1998).

Acknowledgements

We thank all of our collaborators and trainees who have contributed either directly or indirectly to the development of MicroED. We thank G. Calero (University of Pittsburgh) for providing Figs. 4c and 5b. The Gonen laboratory is supported by funding from the Howard Hughes Medical Institute (HHMI). The Nannenga laboratory is supported by the US National Institutes of Health (R01GM124152). MicroED was developed at the Janelia Research Campus of HHMI using HHMI funds and Janelia Visitor Program funds.

Competing interests

The authors declare no competing interests.

Additional information

Reprints and permissions information is available at www.nature.com/reprints.

Correspondence should be addressed to B.L.N. or T.G.